

# Wavelength calibration of spectra measured by the Global Ozone Monitoring Experiment by use of a high-resolution reference spectrum

Jos H.G.M. van Geffen *and* Roeland F. van Oss

Royal Netherlands Meteorological Institute (KNMI)  
P.O. Box 201, 3730 AE De Bilt, The Netherlands

Published in: *Applied Optics* **42**, 2739–2753, 2003.

---

## Abstract

Earthshine spectra measured by the nadir-viewing Global Ozone Monitoring Experiment (GOME) spectrometer aboard the ERS-2 satellite in the range 240–790 nm are widely in use for the retrieval of concentrations and vertical profiles of atmospheric trace gases. For the near-real time delivery of ozone columns and profiles at KNMI, a tailor-made wavelength calibration method was developed. The method uses a high-resolution (0.01 nm) solar spectrum as reference spectrum and applies both a shift and a squeeze to the wavelengths in selected windows to find the optimal wavelength grid per window. This provides a calibration accuracy of 0.002 nm below and 0.001 nm above 290 nm. The new wavelength calibration method can be used on any wavelength window, for example to improve the calibration of spectra from the GOME Data Processor (GDP). A software package called GomeCal which performs this re-calibration, along with an improved polarisation and radiometric correction, has been made and is released via the WWW. The method can be used for any high-resolution (ir)radiance spectrometer, such as the satellite instruments SCIAMACHY, OMI and GOME-2.

*OCIS codes:* 010.1290, 120.6200, 280.0280, 300.6170.

---

## 1. Introduction

The Global Ozone Monitoring Experiment (GOME) aboard the ERS-2 (European Remote Sensing) satellite is a nadir-viewing ultraviolet and visible spectrometer. It measures the spectra of sunlight scattered in the atmosphere and reflected by the surface of the Earth. GOME measures in a wide wavelength range: about 240 to 790 nm, divided in four spectral channels (see Table 1). Once a day direct solar spectra are measured for radiometric calibration. The ERS-2 satellite, launched on 21 April 1995 by the European Space Agency (ESA), orbits Earth in a sun-synchronous polar orbit at an altitude of about 790 km. Each orbit takes about 100 minutes, and ERS-2 completes 14 orbits a day. The satellite crosses the equator going north to south at 10:30 a.m. local time.

GOME is equipped with a scan mirror that redirects the backscattered light onto its optical bench. The mirror performs a 4.5-second forward scan from east to west, followed by a 1.5-second backscan from west to east. The largest off-nadir

**Table 1** Wavelength ranges of the four detector channels of the GOME instrument, the approximate detector pixel size and the spectral resolution of GOME for each channel. The last column shows the number of data points (detector pixels) for each channel in GDP level-1 spectra.

| channel | wavelength range | pixel size | resolution | #points |
|---------|------------------|------------|------------|---------|
| 1       | 237 – 315 nm     | 0.11 nm    | 0.17 nm    | 695     |
| 2       | 313 – 405 nm     | 0.12 nm    | 0.17 nm    | 841     |
| 3       | 407 – 608 nm     | 0.22 nm    | 0.30 nm    | 1024    |
| 4       | 599 – 794 nm     | 0.22 nm    | 0.35 nm    | 1024    |

scan angle is about  $30^\circ$ , giving a full swath width of about 960 km at ground level. With this scanning mode, global coverage is achieved in three days. The forward scan is divided into three 1.5-second scan pixels: east, centre (or: nadir) and west (where the centre pixel is directly below the satellite and east and west are relative to centre). In the direction of flight, each ground pixel measures 40 km. For more information on the GOME instrument, the reader is referred to Ref. 1-3 and references therein.

The spectra of scattered or reflected sunlight, the earthshine spectra, contain information on the distribution of various constituents of the Earth's atmosphere. GOME's main objective is to monitor the distribution of ozone. Vertical ozone profiles, for example, can be derived from the spectra at wavelengths between 265 and 330 nm, and total ozone columns from the range 320–340 nm. Cloud fraction and cloud top pressure for the scene of the ground pixel — information necessary for the retrieval of ozone, as clouds shield part of the ozone column from the satellite — are derived from oxygen absorption features in the earthshine spectra, notably the oxygen-A band centred around 762 nm. Apart from ozone, the spectra contain information on a number of other trace gases, such as  $\text{NO}_2$ ,  $\text{SO}_2$ , and  $\text{BrO}$ , as well as of aerosols. Measuring the concentration of these trace gases and their distribution, both horizontally and vertically, is essential for understanding variations in the atmospheric composition, chemical reactions and dynamical processes taking place in the atmosphere and, at a higher level, an understanding of climate change.

### 1.1 GOME Fast Delivery Service

Solar and earthshine spectra, the so-called level-1 data, are the official product release of the GOME Data Processor (GDP) of the ESA Processing and Archiving Facility at DLR (Deutsches Zentrum für Luft- und Raumfahrt) in Oberpfaffenhofen, Germany, together with some level-2 data, *e.g.* the total column of ozone and  $\text{NO}_2$ , and cloud information.<sup>1,4,5</sup> These data are released on CD-ROMs and via the Internet between two weeks and two months after observation.

For monitoring specific phenomena that change quickly with time (such as the "ozone hole" that appears over Antarctica in the austral spring) and special short-term events (such as "ozone mini-holes"; see *e.g.* Ref. 6), as well as for ozone data to be useful for improving numerical weather forecasts and for validation campaigns, it is essential that the ozone data are available on a near-real time basis: within 3 to 6 hours after observation.

**Table 2** Definition of the nine EGOI windows since June 1998, used for the near-real time Fast Delivery Service at KNMI as outlined in the Introduction. The fourth column lists the number of data points (detector pixels) in each window, which totals to 445.

| window | wavelength range   | width    | #points | band |
|--------|--------------------|----------|---------|------|
| 1      | 272.16 – 275.91 nm | 3.75 nm  | 35      | 1a   |
| 2      | 282.93 – 285.55 nm | 2.62 nm  | 25      | 1b   |
| 3      | 292.51 – 302.96 nm | 10.45 nm | 98      | 1b   |
| 4      | 305.31 – 307.87 nm | 2.56 nm  | 25      | 1b   |
| 5      | 311.92 – 314.46 nm | 2.54 nm  | 25      | 1b   |
| 6      | 323.13 – 336.22 nm | 13.09 nm | 116     | 2b   |
| 7      | 351.64 – 352.76 nm | 1.12 nm  | 11      | 2b   |
| 8      | 372.32 – 373.42 nm | 1.10 nm  | 11      | 2b   |
| 9      | 758.00 – 778.50 nm | 20.50 nm | 99      | 4    |

To this end, a GOME Fast Delivery Service (FDS) has been set up at the Royal Netherlands Meteorological Institute (KNMI), which provides total ozone columns, vertical ozone profiles, assimilated ozone fields, UV index forecasts, and cloud data to users via the World Wide Web ([http://www.knmi.nl/gome\\_fd/](http://www.knmi.nl/gome_fd/)). To make the FDS possible, KNMI receives via ftp the part of the raw (level-0) GOME spectra that is available in near-real time: the so-called Extracted GOME Instrument header (EGOI) data, used by ESA to monitor the status of the GOME instrument.<sup>7,8</sup>

The raw data in these EGOIs contain the spectral measurements of nine selected wavelength windows, listed in Table 2, as well as all instrument health parameters, such as system temperatures, and polarisation information. The nine wavelength windows are selected to monitor the detector's status and to provide data to retrieve ozone columns and vertical ozone profiles with sufficient accuracy. Note that detector channels 1 and 2 are divided into two bands ('a' and 'b') for earthshine spectra. The wavelength of the division point between bands 1a and 1b has been changed once since the launch of ERS-2: initially the division was around 307 nm, since June 1998 it is around 283 nm. Band 1a has an integration time of 12 seconds, to improve the signal-to-noise ratio of the spectra. All other bands have an integration time of 1.5 seconds. This implies that band 1a actually comprises two full scans, each with three forward and one backscan pixel, and that the measurement corresponds to a ground pixel of about 960 by 100 km.

EGOI window 6 is the "ozone DOAS window" (Differential Optical Absorption Spectroscopy) from which the total ozone column can be retrieved.<sup>7,9</sup> Windows 1 through 6 are used for the retrieval of ozone profiles.<sup>10</sup> The measurements in windows 7 and 8 are used for the correction of the polarisation sensitivity of the instrument. Window 9 contains the oxygen-A band, which is used for the retrieval of cloud fraction and cloud top height. In FDS, the latter is done with FRESCO (Fast Retrieval Scheme for Cloud Observables<sup>11,12</sup>).

## 1.2 Wavelength calibration

Starting from the raw data sent to Earth by GOME, a number of steps have to be taken to produce spectral data (level-1) from which useful information can be retrieved.<sup>13</sup> One of these steps is a wavelength calibration, linking each detector pixel to a specific wavelength. The standard wavelength calibration of the GDP uses spectral lines of an onboard PrCr/Ne hollow cathode lamp to correct for shifts in the wavelengths associated with the detector pixels, for example caused by temperature effects, with respect to a pre-flight calibration. The calibration lamp provides a large set of emission lines throughout GOME's wavelength range<sup>1,2</sup>, though the coverage is sparse in some parts of the spectral range.

The calibration method has proved to be insufficiently accurate for the retrieval of ozone profiles, which requires an accuracy in the wavelength calibration of about 0.002 nm, and the accuracy of the DOAS-column retrieval of trace gases also improves with a more accurate wavelength calibration, as shown by sensitivity studies done for the Ozone Monitoring Instrument (OMI).<sup>14</sup> Similar sensitivity studies have not been performed for GOME, but the results of the studies for OMI and some simple test-case studies have shown that the quality of most retrieved level-2 products can be expected to improve with an improved wavelength calibration. Since the retrieval depends on several factors, it is not possible to give an quantitative statement on the improvement a good wavelength calibration makes.

Apart from the observed insufficient accuracy of the GDP calibration method, there are indications that the calibration lamp is malfunctioning, and it may therefore be necessary to switch it off permanently. For these reasons, a new calibration method has been developed for the FDS. The method — which is described in Section 2 — uses as reference spectrum a high-resolution solar spectrum, with irradiance values given at 0.01-nm intervals. This spectrum<sup>15</sup> has been obtained from ground-based and balloon-based measurements with an accuracy of 0.001 nm above 300 nm and 0.002 nm below that.

To better match GOME observations against this reference spectrum, the latter is convolved with GOME's slit function and subsequently integrated over the spectral bins of the detector. The location and width of these bins are allowed to vary along the detector: both a shift and a squeeze are applied to the measurements (the GDP's calibration method with the lamp lines applies only a shift). Starting from an initial guess of the wavelength grid, each of the nine EGOI windows is calibrated separately. The method is akin to the chi-square minimisation of a merit function investigated by Caspar and Chance<sup>16</sup>, who used a general least-square fitting procedure. The method described in the present paper employs a tailor-made chi-square minimisation, and applies both a shift and a squeeze.

Section 3 discusses some important issues regarding the calibration, such as the accuracy of the calibration and the required signal-to-noise ratio of the spectra, and looks briefly at the variation of the calibration results along an orbit and from orbit to orbit.

The calibration method was initially specifically designed for use with the EGOI windows in the level 0-to-1 processor of the FDS. It can, however, be used also to re-calibrate the wavelength grid of GDP level-1 spectra, as the method

can be applied to any wavelength window within the range of the reference spectrum. For this reason, the method has been implemented as part of a software package called GomeCal, which also includes an improved polarisation correction as well as a re-calibration of the reflectivity and a correction for the degradation of the GOME instrument. The package, which is introduced in Section 4, is made available via the World Wide Web ([http://www.knmi.nl/gome\\_fd/gomecal/](http://www.knmi.nl/gome_fd/gomecal/)).

Finally, some concluding remarks are given in Section 5.

## 2. The wavelength calibration method

The wavelength calibration method employs a high-resolution reference spectrum and performs a non-linear fit of two parameters: a shift and a squeeze, which are defined with respect to some initial wavelength grid. The method determines the shift and squeeze — and hence the wavelength grid — that has the smallest ( $\chi^2$ ) difference between the measured and a simulated GOME spectrum. The latter is constructed from the reference spectrum and the instrument slit function.

### 2.1 The reference spectrum

The reference spectrum is a solar spectrum<sup>15</sup> which has irradiance values given at 0.01 nm sampling and which is constructed from ground-based and balloon-based measurements. This spectrum is a suitable reference spectrum for the wavelength calibration, since the spectral structure of the Fraunhofer lines is also present in GOME's solar and earthshine spectra. The reference spectrum is calibrated in the range 300-800 nm to an absolute accuracy of 0.001 nm; for wavelengths in the range 235-300 nm the accuracy is about 0.002 nm.

The same reference spectrum was used by Caspar and Chance<sup>16</sup> for wavelength calibration studies. As these authors note, the reference spectrum also contains some atmospheric lines, which are useful for the calibration of the reference spectrum itself and may assist in the calibration of the GOME earthshine spectra. Some of the atmospheric features, however, dominate over the Fraunhofer lines and these are therefore not suitable for the calibration method discussed in this paper, notably the oxygen-A band in window 9 (see Section 3.1). The ozone absorption features in window 6, used for the DOAS-retrieval of ozone columns, cause no such problems as the Fraunhofer lines clearly dominate the spectrum.

For the calibration of a certain wavelength window, a part of the reference spectrum is taken which is 1 nm wider on either side of the window. The reference spectrum  $S_{\text{ref}}(\lambda)$  is degraded to GOME's resolution with the instrument slit function  $F$ , which is a normalised flat-topped Gaussian-like function.<sup>4</sup> The convolved reference spectrum is then integrated over the spectral bins of the detector and normalised by the wavelength interval (pixel-binning). Figure 1 is an example of the reference spectrum and the convolved spectrum to be used for the calibration of window 1 before the pixel-binning step.

The convolved and pixel-binned reference spectrum  $S(\lambda(j))$  at detector pixel  $j$  with central wavelength  $\lambda(j)$  is given by:

$$S(\lambda(j)) = \int d\lambda' \int d\lambda'' F(\lambda', \lambda'') S_{\text{ref}}(\lambda'') , \quad (1)$$

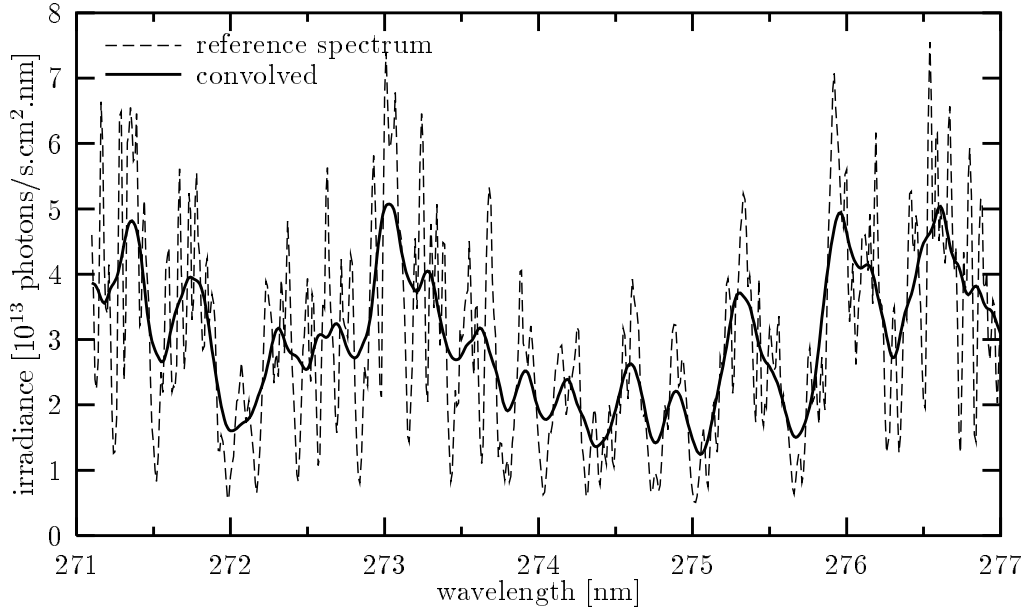


**Figure 1** Reference spectrum for the wavelength calibration of window 1 at 0.01 nm resolution, and the reference spectrum after convolution with GOME's slit function.

where the  $\lambda'$ -integration is over the width of pixel  $j$  and the  $\lambda''$ -integration is over the full range of the slit function. The GOME slit function  $F$  has a FWHM (full-width half-maximum) resolution of 0.17 nm for windows in channels 1 and 2, and 0.35 nm for channel 4 (*cf.* Table 1), and it is assumed that  $F$  has the same shape for all four channels. The convolved and pixel-binned reference spectrum  $S(j) \equiv S(\lambda(j))$  for the calibration is henceforth simply referred to as the reference spectrum.

## 2.2 The wavelength grid

The wavelength grid used in the calibration method is, for a given channel, given by a fifth-degree polynomial:

$$\lambda(j) = a_1 + a_2j + a_3j^2 + a_4j^3 + a_5j^4, \quad (2)$$

where  $\lambda(j)$  is the wavelength at the centre of detector pixel  $j$ , with  $j = 0$  for the first pixel and  $j = M - 1$  for the last pixel of the channel under consideration, where  $M$  is the number of detector pixels of the channel and is given in the last column of Table 1. This parameterisation is sufficient to describe GOME's wavelength grid and is also used in the GDP. The coefficients  $a_k$  in Eq. (2) are different for the four channels and hence should be denoted as  $a_k^n$  for channel  $n$ , but for brevity the upper index is omitted.

Figure 2 shows for window 1 the convolved and pixel-binned reference spectrum (*cf.* Figure 1) and a GOME solar spectrum of 2 June 2000 on the wavelength grid given by the GDP. Both spectra are dimensionless and have been suitably scaled; this aspect of the method is discussed below in Section 2.4.

The wavelength calibration method adjusts the first and second coefficient of the polynomial such that the best fit between the measured and the reference

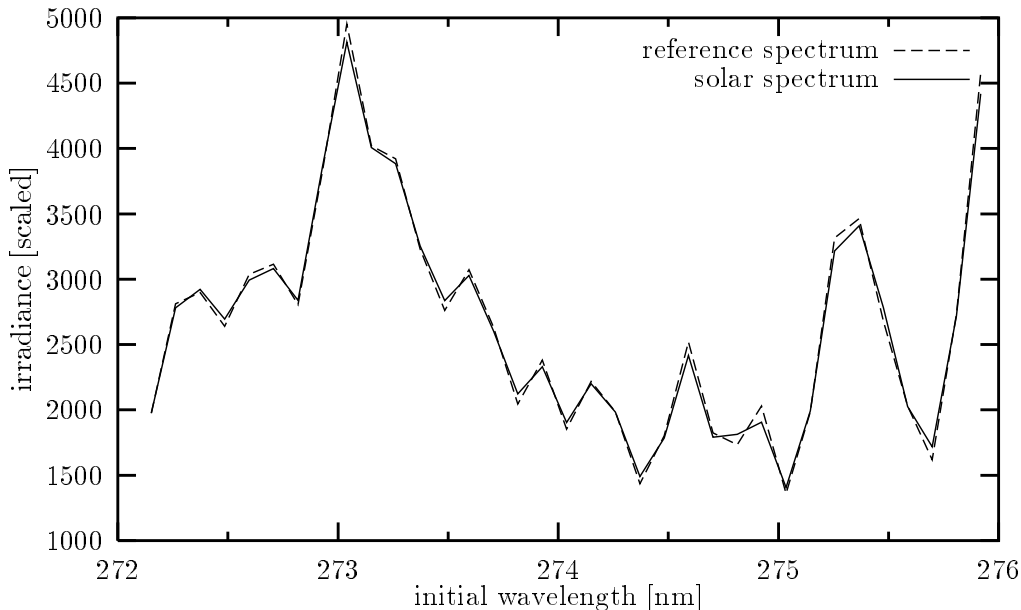


**Figure 2** Reference spectrum and measured solar spectrum in window 1, as function of the initial wavelength grid, before the calibration procedure has started. The solar spectrum was measured on 2 June 2000. The spectra are dimensionless and have been scaled in the manner discussed in Section 2.4.

spectrum is achieved. This entails applying a shift ( $\alpha$ ) and squeeze ( $\beta$ ) to the wavelength grid given by Eq. (2) for each window separately, forming new wavelengths:

$$\lambda'(j) = (a_1 + \alpha) + (a_2\beta)j + a_3j^2 + a_4j^3 + a_5j^4 . \quad (3)$$

Note that the shift is a wavelength increment and has as dimension [nm], while the squeeze is a correction to the width of the spectral pixel and is a dimensionless factor.

Because of a combination of both shift and squeeze in the calibration, the change of wavelength with respect to the initial guess is different for each detector pixel in the window being calibrated:

$$\Delta\lambda(j) = \lambda'(j) - \lambda(j) = \alpha + a_2(\beta - 1)j , \quad (4)$$

with the combination ( $\alpha = 0, \beta = 1$ ) representing no change in the wavelength grid.

### 2.3 The calibration procedure

Denote the measured earthshine or solar spectrum that is to be calibrated by  $G(i)$ , with  $i = 1, \dots, N$  the data points within the window under consideration, and  $\delta G(i)$  the error on  $G(i)$ ; both  $G(i)$  and  $\delta G(i)$  are obtained from the measurements and are input to the wavelength calibration procedure. Further let  $S(i)$  represent the reference spectrum, pixel-binned at the same wavelength grid. The latter is a function of the shift and squeeze applied with respect to the initial grid (given by Eq. (2)) and hence  $S(i) = S(i, \alpha, \beta)$ . In essence, the wavelength calibration is a

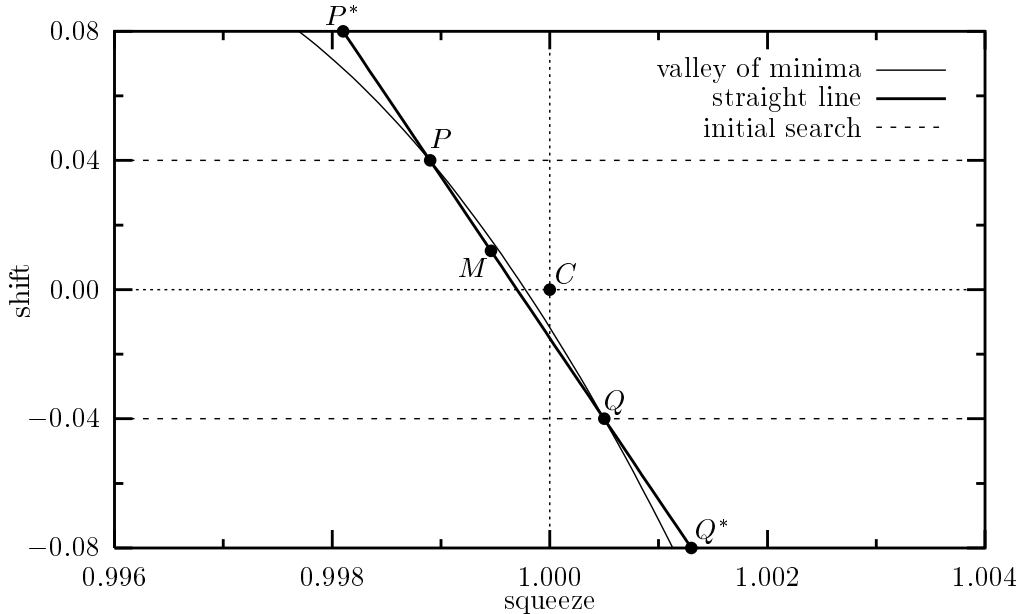


**Figure 3** Schematic illustration of the wavelength calibration method in the shift-squeeze-plane. The shift has as dimension nm, the squeeze is a dimensionless factor. See the text of Section 2.3 for an explanation of the lines and points in the graph.

minimisation of a  $\chi^2$  merit function:

$$\chi^2(\alpha, \beta) = \frac{1}{N-2} \sum_{i=1}^N \left[ \frac{G(i) - S(i, \alpha, \beta)}{\delta G(i)} \right]^2, \quad (5)$$

where the factor  $N - 2$  is due to the reduction of the degrees of freedom by two. Note that the spectra in Eq. (5) are in dimensionless units and suitably scaled (see Section 2.4). The remainder of this subsection describes in some detail the method to find the minimum  $\chi^2$ -value; the accuracy of the method is discussed in Section 3.5.

From the wavelength difference per pixel in the window, given by Eq. (4), it is clear that a range of  $(\alpha, \beta)$ -combinations gives more or less the same  $\Delta\lambda$ -values and hence more or less the same  $\chi^2$ -values. For each shift-value one can find a squeeze that minimises Eq. (5). Connecting all these minima thus gives a valley of  $\chi^2$ -minima in the  $\alpha, \beta$ -plane and somewhere within that valley is the absolute minimum the calibration method is looking for.

Figure 3 shows schematically the  $\alpha, \beta$ -plane to outline the calibration method. The valley of  $\chi^2$ -minima is a slightly curved line in this plane, shown by the thin solid line in the figure. The valley is curved with respect to a straight line either to the left or to the right (which orientation is unknown in advance), but with a curvature that is in general not as big as sketched in Figure 3. In all the calibrations used for setting up and testing the method, the line is tilted as in Figure 3: for positive shift values the squeeze is less than unity, and for negative shift values the squeeze is larger than unity, at some distance from the centre point  $C \equiv (\alpha = 0, \beta = 1)$ . Whether the valley of minima passes to the left or right of  $C$  at the no-shift line is not known in advance: it varies from case to case.

The  $\alpha, \beta$ -domain in which to search has to be limited, else the search may lead to unacceptable results. The initial wavelength grid is expected to be already fairly good: the wavelength change  $\Delta\lambda$  due to the calibration is assumed to be less than the width of a pixel. For this reason the value of the  $\alpha$ -parameter is limited to the interval  $\pm 0.08$  nm shown in Figure 3. The actual change  $\Delta\lambda(i)$  depends on the  $\beta$ -value found, as Eq. (4) shows. In all cases studied,  $\beta$  was well within the range (0.996, 1.004) depicted in Figure 3.

Searching for the minimum  $\chi^2$ -value of Eq. (5) in the  $\alpha, \beta$ -plane can in principle be done using a standard two-dimensional search routine. Such a method has, however, a drawback: the search may not be very efficient as the valley of minima has a rather flat bottom, *i.e.* the gradients in  $\chi^2(\alpha, \beta)$  are not very large. A more efficient search method has been devised: first determine two points of the valley of minima, then search for the minimum along the valley. Since the valley of minima is only slightly curved, as in Figure 3, it can be approximated rather well by a straight line, and searching for a minimum along a straight line can be done efficiently with standard numerical routines.<sup>17</sup>

The following search procedure is adopted. First the minimum along the line  $\alpha = +0.04$  nm (mid-way the allowed  $\alpha$ -range), for which  $\beta < 1$  is expected, is found at point  $P$  (in terms of Figure 3). Then the minimum along the line  $\alpha = -0.04$  nm, for which  $\beta > 1$ , is found at  $Q$ . The straight line  $PQ$  is extended to  $\alpha = \pm 0.08$  nm, *i.e.* to  $P^*Q^*$ , and used to represent the valley of  $\chi^2$ -minima. Since this valley is slightly curved, fixing the straight line at  $\alpha = \pm 0.08$  nm (instead of at  $\alpha = \pm 0.04$  nm) would give a less accurate representation of the valley of minima.

The next step is to search along the straight line  $P^*Q^*$  for the minimum  $\chi^2$ -value:  $\chi_1^2(\alpha_1, \beta_1)$  at, say,  $M$  in Figure 3. Since the straight line is a fairly good representation of the valley of  $\chi^2$ -minima, the  $(\alpha_1, \beta_1)$ -pair is the result of the first iteration step in the calibration procedure. But since the valley of minima is in reality slightly curved, this result is not the exact minimum.

Next, the initial wavelength grid is adapted with  $(\alpha_1, \beta_1)$  and the search process is repeated in a domain like the one in Figure 3 but centred around  $(\alpha_1, \beta_1)$ :  $P$  and  $Q$  are determined again, etc., leading to a new minimum  $\chi_2^2(\alpha_2, \beta_2)$ . If  $\chi_2^2 > \chi_1^2$ , the new minimum is not an improvement and the  $(\alpha_1, \beta_1)$ -pair is taken as the result of the whole calibration procedure. If on the other hand  $\chi_2^2 < \chi_1^2$ , the new minimum is an improvement and the procedure is repeated for a third iteration step, leading to  $\chi_3^2(\alpha_3, \beta_3)$ .

In fact, the convergence criterion is as follows:

$$\begin{aligned} (\chi_{k+1}^2 - \chi_k^2)/\chi_k^2 > 0 & : \quad \chi_k^2 \text{ accepted} \\ -\epsilon < (\chi_{k+1}^2 - \chi_k^2)/\chi_k^2 < 0 & : \quad \chi_{k+1}^2 \text{ accepted} \\ (\chi_{k+1}^2 - \chi_k^2)/\chi_k^2 < -\epsilon & : \quad \text{next iteration step} \end{aligned} \quad (6)$$

with  $\epsilon = 0.01$  (a smaller value does not significantly alter the  $\Delta\lambda$  found from the calibration but takes more computational time). The maximum number of iteration steps is set at five. For the vast majority of GOME earthshine spectra and all solar spectra considered, two or three iteration steps sufficed to find the lowest  $\chi^2$ -value. A fifth iteration step is required for several calibrations of windows 7 and

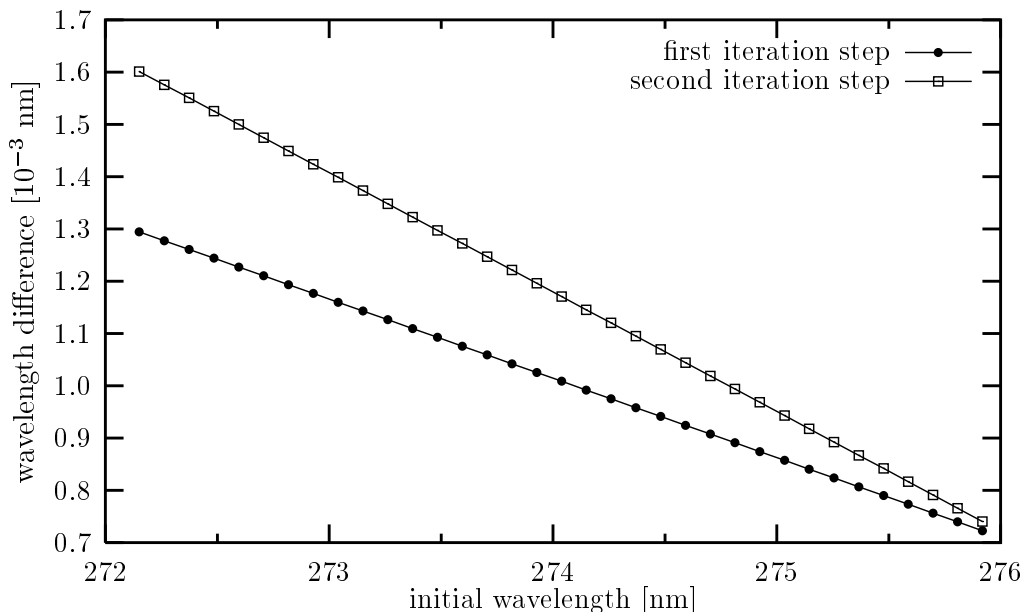


**Figure 4** Wavelength difference  $\Delta\lambda$  in  $10^{-3}$  nm as a result of the first and second iteration steps in the calibration of the solar spectrum plotted in Fig. 2 as a function of the initial wavelength values.

8 (presumably because of the small number of data points); further computations in these cases yielded no significant improvements in the shift and squeeze values of the minimum.

Points  $P$  and  $Q$  in Figure 3 can be found in all cases, hence the straight line  $P^*Q^*$  is always defined. If the spectral data are of poor quality, it may happen that a minimum cannot be found between  $P^*$  and  $Q^*$ , *i.e.* the function  $\chi^2(\alpha, \beta)$  is monotonic along that line. Extending the search beyond  $P^*$  and  $Q^*$ , however, might lead to unacceptably large  $\Delta\lambda$ -values with respect to the detector pixel size. For that reason, if no minimum is found on  $P^*Q^*$ , the calibration method sets  $\beta = 1$  and searches for a minimum along that line:  $M'(|\alpha| \leq 0.08, \beta = 1)$ , which is then considered the best possible minimum. If along the line  $\beta = 1$  a minimum cannot be found (when the quality of the data is really poor), the shift is also turned off and the initial wavelength grid is the final grid.

As an example, consider the calibration of the solar spectrum plotted in Figure 2. At the initial wavelength grid ( $\alpha = 0, \beta = 1$ ) shown in that graph  $\chi_0^2 = 83.7889$ . For the first iteration step the results of the calibration are  $\alpha_1 = 0.006371$  nm and  $\beta_1 = 0.999864$ , with  $\chi_1^2 = 83.0741$ . The second iteration step in the calibration results in  $\alpha_2 = 0.009247$  nm and  $\beta_2 = 0.999796$ , with  $\chi_2^2 = 82.9141$ . The respective wavelength changes for both iteration steps are plotted in Figure 4 as function of the initial wavelength grid. The relative difference in  $\chi^2$  between the first and second iteration step  $(\chi_2^2 - \chi_1^2)/\chi_1^2$  is  $-0.0019$ , which implies that the results from the second iteration step are accepted and the calibration procedure is ended for this window.

Figure 5 shows the elements of the  $\chi^2$ -computation of the final iteration step. The solid line is the difference between measured and reference spectrum, *i.e.* the difference between the two curves of Figure 2, but now on the final wavelength grid.

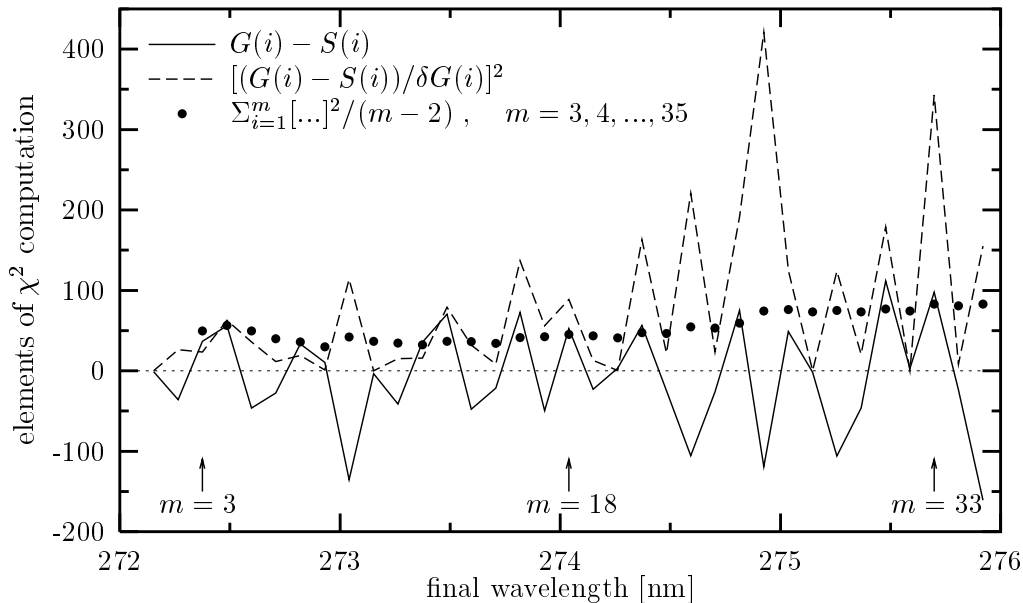


**Figure 5** Elements of the computation of  $\chi^2$  of the second iteration step for the example in Section 2.3 of window 1 in a solar spectrum (cf. Fig. 2) on the final wavelength grid. For an explanation of the curves, see the text.

The dashed line shows the individual terms of the summation of  $\chi^2$ , cf. Eq. (5), where the error  $\delta G(i)$  varies between about 4 and 13 on this scale. Clearly, at some points in the window the match is much better than at other points. The filled circles in the graph show the "running" computation of  $\chi^2$ , that is: the value of  $\chi^2$  from the left (point  $i = 1$ ) to the right, up to and including point  $m = 3, 4, \dots, N$ , with  $N = 35$  (cf. Table 2).

A  $\chi^2$ -value of 83 appears to be a large value. Ideally, the calibration result is such that the reference spectrum  $S(i)$  at the final wavelength grid represents the measured spectrum  $G(i)$  to the level of the error  $\delta G(i)$  in the measurement, in which case  $\chi^2$  would be about unity. In this example, the measured spectrum is a solar spectrum and so is the reference spectrum, and hence one might expect a good match. The reason for the apparent remaining mismatch is a combination of several aspects. The true solar spectrum at the moment of the measurement may differ from that of the reference spectrum, as the solar spectrum varies somewhat with time. There are some atmospheric features in the reference spectrum that are not present in the measured solar spectrum. Furthermore, the error  $\delta G(i)$  in the measurements may be underestimated.

More importantly, both the shape and the resolution of the slit function (function  $F$  in Eq. (1) and its FWHM) may be inaccurate. In fact, looking at the difference in the sharpness of the individual peaks of the spectra in Figure 2 suggests that the resolution of the slit function is somewhat too small for this case. Increasing the resolution in steps of 0.005 nm for this window results first in a decrease and then in an increase of  $\chi^2$ , with a minimum value of 30.7096 at a resolution of 0.190 nm. For the other windows, increasing the resolution somewhat from the values listed in Table 1 may increase or decrease  $\chi^2$  or have little effect on  $\chi^2$ . Evidently, each wavelength window has its own optimal resolution. Yet it is unclear whether the minimum of  $\chi^2$  is a good indicator for the correct

resolution value. Window 2, for example, shows a continuously decreasing  $\chi^2$  for increasing resolution in the range tested (0.150 – 0.190 nm), whereas window 5 shows a continuous increase of  $\chi^2$  in that range.

When calibrating earthshine spectra, the remaining mismatch between reference and measured spectrum is larger, giving larger  $\chi^2$ -values, since an earthshine spectrum contains more pronounced atmospheric absorption features than the reference spectrum. The polynomial scaling of the measured spectrum, discussed in Section 2.4, removes the broad-scale structures of atmospheric absorption and scattering in  $G(i)$ , that is: the part of the absorptions which varies slowly with wavelength. Atmospheric features varying relatively fast with wavelength are not removed by the scaling and thus cause mismatches with the reference spectrum.

## 2.4 Scaling the spectra

Minimisation of Eq. (5) can be performed well only if the measured and reference spectra have values of the same order. If the difference between these spectra is large, then this difference overshadows the relatively small difference due to a mismatch in the wavelengths. A suitable scaling of the spectra is therefore essential, in particular to remove the broad-scale atmospheric features, which are strongest for the shortest wavelengths.

The wavelength calibration in the FDS level 0-to-1 processor is done before physical units are assigned to the spectral value and hence the spectra are dimensionless (assigning units is done after the calibration and is a simple multiplication by a scaling factor). The numerical value of the spectra to be calibrated is of the order of  $10^3$ , whereas the reference spectrum has numerical values of the order of  $10^{14}$  (*cf.* Figure 1). Hence, the first scaling step is dividing the reference spectrum by  $10^{10}$  photons/s.cm<sup>2</sup>.nm. The scaled reference spectrum is the dimensionless variable  $S(i)$  in Eq. (5).

In the following  $G^*(i)$  denotes the unscaled dimensionless measured spectrum and  $G(i)$  represents the scaled dimensionless spectrum in Eq. (5).

For the calibration to work well, a more detailed scaling must be performed on the measured spectrum  $G^*(i)$  to give it an average value similar to  $S(i)$ . For a measured solar spectrum a simple constant factor  $c_1$  may be sufficient,  $G(i) = c_1 G^*(i)$ , as the reference spectrum is also a solar spectrum. For an unscaled earthshine spectrum, however, a more complicated scaling is required:  $S(i)$  and  $G^*(i)$  not only differ in average value, but there is also a difference in the average slope of the spectra as function of wavelength.

Figure 6 shows for window 3 the reference spectrum (solid line) together with a measured solar spectrum (dashed line) before any further scaling, and a measured earthshine spectrum (dotted line) which has been multiplied by 200 to give it roughly the same value as the other spectra. (The earthshine spectrum is actually an average over 10 spectra, as is usual for the FDS; see Section 3.5.)

The variation with wavelength of the (ir)radiance levels of the spectra in Figure 6 is different: the reference spectrum shows a gradual decrease in irradiance level for increasing wavelength, whereas the radiance of the earthshine spectrum gradually increases. A simple constant or linear scaling of  $G^*(i)$  is therefore insuf-

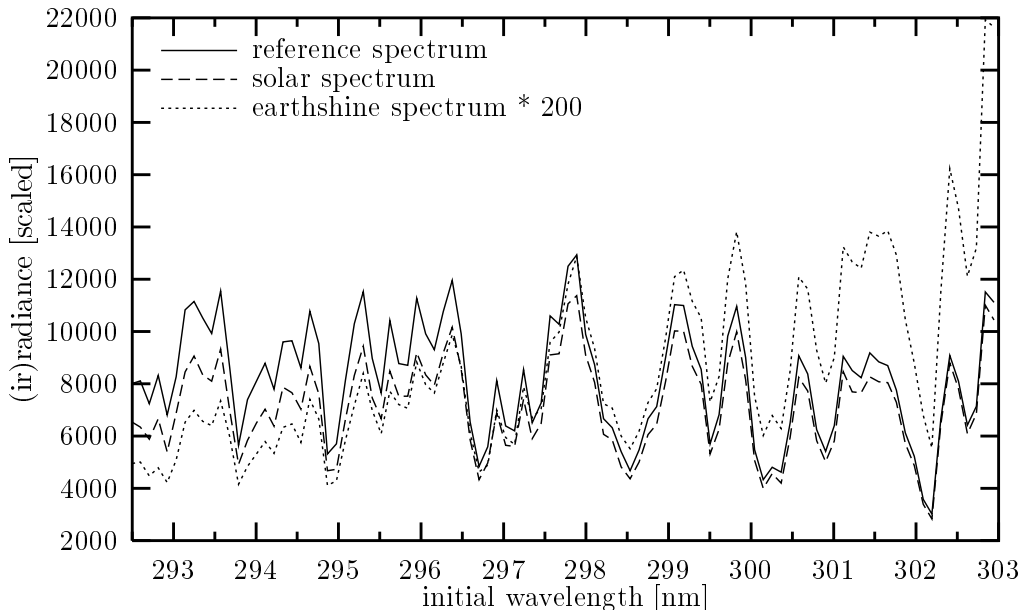


**Figure 6** Reference spectrum for the wavelength calibration of window 3, a measured solar spectrum, and a measured earthshine spectrum, which is multiplied by 200 for accommodation on the same vertical scale. The solar spectrum is from 2 June 2000, and the earthshine spectrum is an average over 10 spectra from the orbit that started around 11:20 GMT that day.

ficient to obtain similar numerical values for measured and reference spectra. For that reason, the scaling is done with a fourth-degree polynomial fit of the following form:

$$\frac{S(i)}{G^*(i)} \xrightarrow{\text{fit}} f(i), \quad f(i) \equiv c_1 + c_2i + c_3i^2 + c_4i^3, \quad (7)$$

with  $i = 0, 1, \dots, N - 1$  the pixel number within the window. The fit results  $c_1, c_2, c_3, c_4$  then give a scaled measured spectrum:

$$G(i) = f(i)G^*(i), \quad (8)$$

and it is this  $G(i)$  that appears in Eq. (5). A fourth-degree polynomial is used here, because a lower degree polynomial gives clearly worse results, whereas a higher degree does not give a significant improvement. Table 3 shows examples of the polynomial scaling: it lists the coefficients of the scaling of the measured solar spectrum shown in Figure 2, as well as the coefficients of the scaling of the measured solar and earthshine spectra in Figure 6.

This polynomial scaling reduces the average difference between the curves of  $S(i)$  and  $G^*(i)$  as a function of wavelength sufficiently for the minimisation of Eq. (5) to proceed. This works for measured solar spectra for all windows and for measured earthshine spectra for windows 3 through 9. For windows 1 and 2 in earthshine spectra, however, the difference between  $S(i)$  and the unscaled  $G^*(i)$  is so large that the polynomial scaling can in some cases (notably when the quality of the spectrum is not too good) remove part of the spectral features, which would then hamper the minimisation of Eq. (5) severely.

To prevent this problem from occurring, a linear scaling is applied before the above fourth-degree polynomial scaling for windows 1 and 2 in earthshine spectra

**Table 3** Example of the fourth-degree polynomial coefficients for the scaling in Eqs. (6,7) of the solar spectra in windows 1 and 3, and of the earthshine spectrum in window 3; the spectra are those plotted in Figures 2 and 6.

| coef. | solar #1                 | solar #3                 | earthshine #3            |
|-------|--------------------------|--------------------------|--------------------------|
| $c_1$ | $+0.2597 \times 10^{+1}$ | $+0.1263 \times 10^{+1}$ | $+0.3390 \times 10^{+3}$ |
| $c_2$ | $-0.2545 \times 10^{-1}$ | $-0.2168 \times 10^{-2}$ | $-0.2597 \times 10^{+1}$ |
| $c_3$ | $+0.2585 \times 10^{-3}$ | $-0.2277 \times 10^{-4}$ | $-0.7882 \times 10^{-2}$ |
| $c_4$ | $+0.3308 \times 10^{-5}$ | $+0.2463 \times 10^{-6}$ | $+0.1031 \times 10^{-3}$ |

only, in the following way. A linear fit is made between the measured earthshine spectrum  $G^*(i)$  and the reference spectrum  $S(i)$ :

$$S(i) \xleftrightarrow{\text{fit}} AG^*(i) + B, \quad (9)$$

and the resulting coefficients  $A$  and  $B$  are used to make a new measured earthshine spectrum:

$$G_{\text{lin}}^*(i) = AG^*(i) + B, \quad (10)$$

after which  $G_{\text{lin}}^*(i)$  is used in Eqs. (6,7), rather than  $G^*(i)$ , for the polynomial scaling.

### 3. Wavelength calibration in the EGOI windows

The wavelength calibration method is described in the preceding section in general terms. This section deals with aspects specific to the calibration of spectra in the nine EGOI windows, in particular the choice of the initial wavelength grid in the FDS and the re-calibration of full level-1 GDP spectra. Further, the accuracy of the calibration method and the presence of a very small systematic offset are discussed; for these investigations simulated spectra are used.

#### 3.1 Wavelength window 9

The earthshine spectrum in window 9 contains absorption features of the oxygen-A band, which are used by the FRESCO algorithm<sup>11,12</sup> in the FDS for the retrieval of cloud top height and cloud fraction in the ground pixel. Figure 7 shows a solar and earthshine spectrum measured by GOME as produced by the GDP, plotted in arbitrary units and scaled such that the absorption features can be compared easily. The horizontal line near the top of the panels indicates the size of window 9. The solar spectrum contains only relatively small features in this wavelength region, at least compared to the depth of the oxygen features in the earthshine spectrum.

Figure 7 also shows the convolved reference spectrum before pixel-binning (dotted line). The reference spectrum clearly has relatively strong oxygen absorption features around 762 nm, which makes this part of the spectrum unsuitable for usage in the wavelength calibration of solar spectra in window 9. Earthshine spectra have the oxygen absorption features. But the left part of the window is not suitable for the calibration of these spectra as the depth of the absorption lines

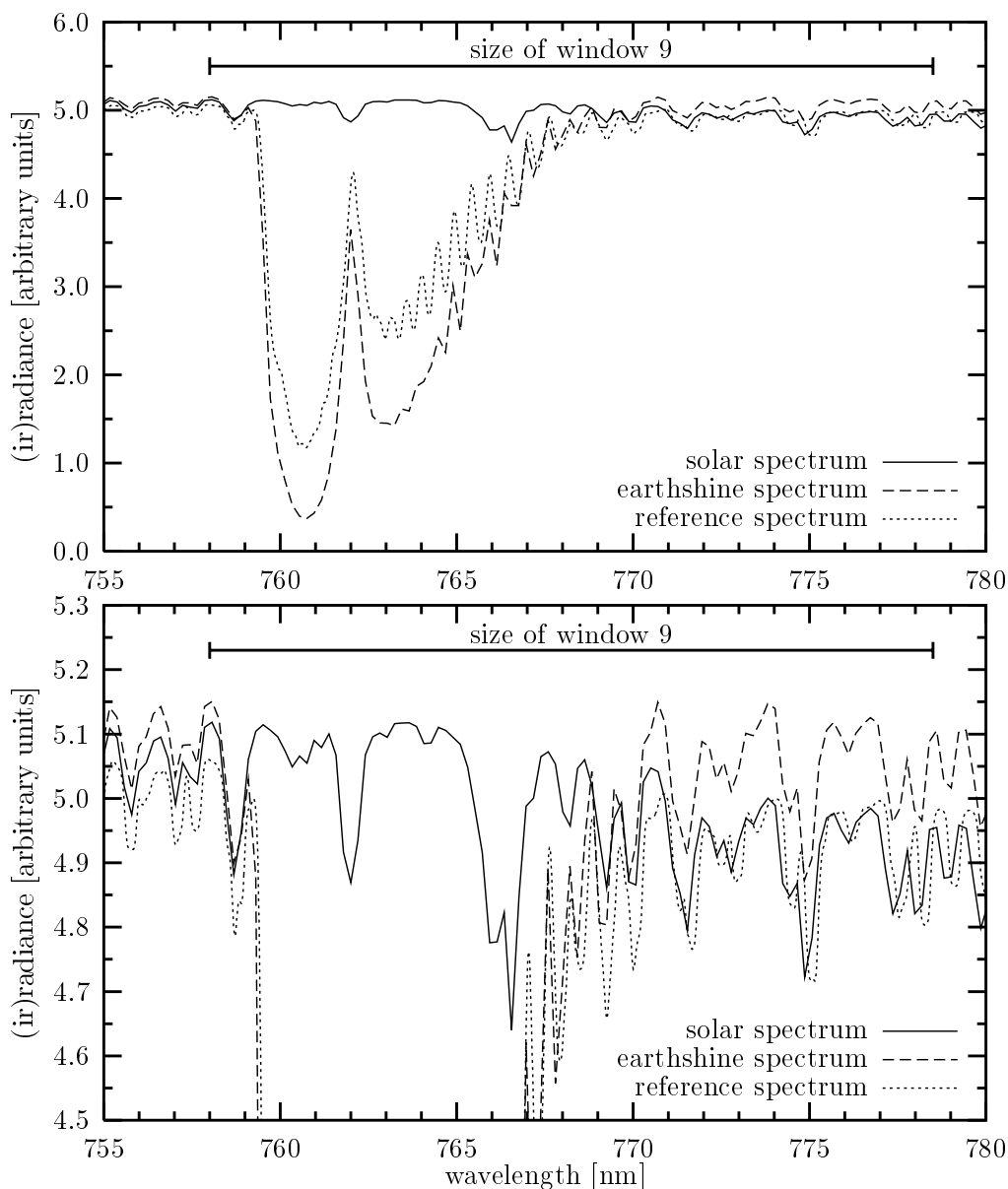


**Figure 7** GDP solar and earthshine spectra around the oxygen-A band, and the convolved reference spectrum, in arbitrary units. The top panel shows the full spectra, the bottom panel an enlargement of the continuum level. The size of window 9 is indicated near the top of the panels.

varies considerably from spectrum to spectrum (depending *e.g.* on the presence of clouds): the large difference in the magnitude of the reference and measured spectra in the oxygen-A band would overshadow the small differences due to mismatches in the Fraunhofer lines.

In the right half of window 9 there are no atmospheric features in the spectra: below 772 nm there are very weak oxygen absorption features,<sup>18</sup> but these are negligible at least down to 768 nm for instruments with a resolution such as GOME has. In this wavelength region a calibration based on the solar absorption features in the reference spectrum is therefore certainly possible. To determine what part of the window is suitable, a set of data points at the right of the window was

used. The number of data points in this set was gradually increased leftwards and the calibration results were monitored. The  $\chi^2$ -value decreases with increasing number of data points, until points in the oxygen-A band are included, at which moment the  $\chi^2$ -value increases abruptly. From this study it appeared that using the part of the spectrum with  $\lambda \geq 768.5$  nm results in a satisfactory calibration.

At the left of the oxygen-A band there is a clear Fraunhofer line around 758.7 nm (see Figure 7), which could in principle be used for the wavelength calibration. Due to the limited resolution in channel 4, however, there are only five or six data points available outside the oxygen-A band (window 9 starts at 758.0 nm), which is insufficient for a proper calibration. Hence, for the FDS calibration of window 9, only the part of the spectrum with  $\lambda \geq 768.5$  nm (data points 51 through 99) is used and the result is expanded to the entire window, for both earthshine and solar spectra. If a complete earthshine or solar spectrum is available, as is the case when re-calibrating GDP-made spectra (*e.g.* with the GomeCal software; see Section 4), then one can, of course, define a wavelength window just to the left and another window immediately to the right of the oxygen-A band and use these to calibrate this part of the spectrum.

### 3.2 Initial wavelength grid

The wavelength grid of the GDP level-1 spectra is described by the fifth-degree polynomial in Eq. (2), with coefficients valid for an entire channel and different for the four GOME channels. For the wavelength calibration method described in Section 2 the initial grid must be within one pixel size of the final grid to make a calibration possible. When re-calibrating GDP level-1 spectra (next subsection) the wavelength grid of the GDP logically serves as initial grid.

For the FDS level 0-to-1 processor, however, such an initial wavelength grid is not available: the measurements in the level-0 data are given at detector pixel numbers, and a wavelength value has to be assigned to each detector pixel. Hence, for the FDS an initial wavelength grid is constructed off-line, on the basis of a re-calibration of the GDP-made solar spectrum measured by GOME on 26 February 1998. Since in the FDS the calibration is performed for each of the windows separately, each window generates its own set of polynomial coefficients. These sets form the initial grids for the wavelength calibration, for both the solar and the earthshine spectra in the FDS.

The wavelength grids thus constructed are in a sense still an arbitrary choice for the initial grid for the individual windows. This implies that the absolute values of the shift and squeeze found by the calibration in the FDS have no physical meaning. By always starting from the same initial grid, however, a comparison of the calibration results for the same window is possible, for example for ground pixels along an orbit or between successive orbits (geographically or in time); see Section 3.7.

### 3.3 Re-calibration of GDP spectra

Using the wavelength calibration method described in Section 2, the level-1 spectra of the GDP can be re-calibrated in specific wavelength windows, for which

**Table 4** Change in the wavelength  $\Delta\lambda(i)$  of the first, middle, and last data points of the nine windows listed in Table 2 due to a re-calibration of the wavelength grid of the GDP solar spectrum at 26 February 1998 and the earthshine spectrum of 04:13:18 GMT at 27 February 1998, both extracted with version 2.00 of the GDP\_01 extractor. For changes that are the same for the three points, no squeeze was applied. Note that the detector pixel size of windows 1 through 8 is about 0.11 nm and of window 9 about 0.22 nm (cf. Table 1).

| win-<br>dow | change in wavelength $\Delta\lambda(i)$ [nm] |           |           |                     |           |           |
|-------------|--|-----------|-----------|---------------------|-----------|-----------|
|             | solar spectrum                               |           |           | earthshine spectrum |           |           |
|             | first  | middle    | last      | first               | middle    | last      |
| 1           | 0.008508                                     | 0.010847  | 0.013048  | 0.001640            | 0.005634  | 0.009392  |
| 2           | 0.018037                                     | 0.018037  | 0.018037  | 0.016818            | 0.016818  | 0.016818  |
| 3           | 0.018477                                     | 0.013953  | 0.009429  | 0.014124            | 0.009290  | 0.004457  |
| 4           | -0.001848                                    | -0.001848 | -0.001848 | -0.002407           | -0.002407 | -0.002407 |
| 5           | -0.062926                                    | -0.064641 | -0.066357 | -0.068860           | -0.070652 | -0.072445 |
| 6           | 0.015796                                     | 0.011276  | 0.006756  | 0.008376            | 0.003599  | -0.001179 |
| 7           | -0.006622                                    | -0.006622 | -0.006622 | -0.008643           | -0.008643 | -0.008643 |
| 8           | -0.006568                                    | -0.006568 | -0.006568 | -0.012274           | -0.012274 | -0.012274 |
| 9           | 0.024535                                     | 0.024535  | 0.024535  | 0.013582            | 0.013582  | 0.013582  |

the GDP's wavelength grid serves as the initial grid for the re-calibration. If the GDP's wavelength grid is correct, the calibration method should give negligible wavelength changes  $\Delta\lambda(i)$  for the detector pixels  $i$  in the windows.

Table 4 lists wavelength changes  $\Delta\lambda(i)$  for the first, middle and last data points when re-calibrating a GDP solar and earthshine spectrum in the nine EGOI windows (cf. Table 2). The data in Table 4 show that in some windows the wavelength calibration of the GDP is rather good, notably in window 4, but in several windows the GDP calibration differs by 0.01 nm or more. It is therefore necessary to re-calibrate GDP level-1 spectra, if an accuracy of 0.01 nm or better is required for a subsequent level 1-to-2 retrieval, *e.g.* of ozone columns and profiles. This re-calibration can be performed with the GomeCal package, introduced in Section 4.

### 3.4 Simulated GOME earthshine spectra

The accuracy of the calibration method presented in this paper is studied by means of simulated GOME earthshine spectrum, made with MODTRAN<sup>19,20</sup> for a centre ground pixel geometry (*i.e.* a viewing zenith angle of 180°), with a solar zenith angle of 20°, a differential azimuthal angle of 0°, a surface albedo of 0.05, and profiles for O<sub>3</sub> and NO<sub>2</sub> typical for a mid-latitude summer situation.

The Kurucz solar spectrum<sup>21,22</sup> in the MODTRAN package was used; this spectrum is given at a wavenumber grid with a step of 1 cm<sup>-1</sup> and a spectral resolution of 5 cm<sup>-1</sup>. The resolution  $R(\lambda)$  of the spectrum therefore varies from  $R(270 \text{ nm}) = 0.036 \text{ nm}$  to  $R(370 \text{ nm}) = 0.068 \text{ nm}$ . This is high enough for simulated spectra in channels 1 and 2 to be suitable for a study of the accuracy of the calibration method, discussed in the next subsection.

For channel 4 the resolution of the spectrum ranges from  $R(600 \text{ nm}) = 0.180 \text{ nm}$  to  $R(795 \text{ nm}) = 0.316 \text{ nm}$ , which is not good enough to study the

accuracy of the method in window 9. But the accuracy of the calibration in channels 3 and 4 is expected to be comparable to the accuracy in channel 2 for a combination of two reasons: the signal-to-noise ratio in GOME's channels 3 and 4 is at least as good as the signal-to-noise ratio in channel 2, and the reference spectrum of the calibration above 300 nm is of very high precision (Section 2.1).

### 3.5 Accuracy of the calibration method

The accuracy of the calibration method is determined by the accuracy of the reference spectrum (Section 2.1) and by the quality of the measured spectrum, *i.e.* by the signal-to-noise ratio. The simulated earthshine spectrum introduced in the preceding subsection is used to study the accuracy. This spectrum constitutes a set of radiance data  $\{\lambda(i), G(i), \delta G(i)\}$  for GOME detector pixels  $i$  over the wavelength range of GOME's channels 1 and 2.

Apart from this "standard spectrum", a series of 25 additional spectra is constructed with a random noise added on the radiance:  $G(i) + r\delta G(i)$ , where  $r$  is a normally distributed random number with zero mean. The signal-to-noise ratio of the earthshine spectra can be improved by averaging  $N_s$  earthshine spectra before the wavelength calibration. The average spectrum is then calibrated and the resulting wavelength grid is applied to the  $N_s$  individual spectra. Note that the averaging is done over consecutively measured earthshine spectra, because the calibration results vary along an orbit and from orbit to orbit (see Section 3.7). For simulated spectra, the averaging is mimicked by dividing the error  $\delta G(i)$  by  $\sqrt{N_s}$ .

The following sets of spectral data are thus used for determining the accuracy of the calibration method for a series of  $N_s$ -values:

$$\left\{ \lambda(i), G(i) + r_k \delta G(i) / \sqrt{N_s}, \delta G(i) / \sqrt{N_s} \right\}, \quad k = 0, 1, 2, \dots, 25 \quad (11)$$

with  $r_0 = 0$ .

Consider the change in wavelength  $\Delta\lambda(i_m)$  of data point  $i_m$  in the middle of the window, as a measure for the accuracy of the calibration of the window. The study shows that for  $k = 0$  the wavelength change does not vary significantly with  $N_s$ : the  $\Delta\lambda$ -values lie within 0.1% (but 0.2% for window 8) of one another.

The accuracy of the calibration method for a given  $N_s$  can therefore be defined as the difference between the wavelength change of the unperturbed spectrum  $\Delta\lambda(i_m, k = 0, N_s)$  and the averaged wavelength change of the 25 perturbed spectra ( $k > 0$ ), plus or minus the standard deviation of this average over 25 spectra,  $\sigma_{25}$ :

$$\text{accuracy} \equiv \max_{\pm\sigma_{25}} \left\{ \left| \Delta\lambda(i_m, k = 0, N_s) - \frac{1}{25} \sum_{k=1}^{25} \Delta\lambda(i_m, k, N_s) \pm \sigma_{25} \right| \right\}. \quad (12)$$

This is a function of  $N_s$ , and clearly the accuracy improves with increasing  $N_s$ : when more spectra are averaged, the better the signal-to-noise ratio, and hence the closer the results of the average over the 25 perturbed spectra are to the results of the unperturbed spectrum. The desired accuracy therefore determines

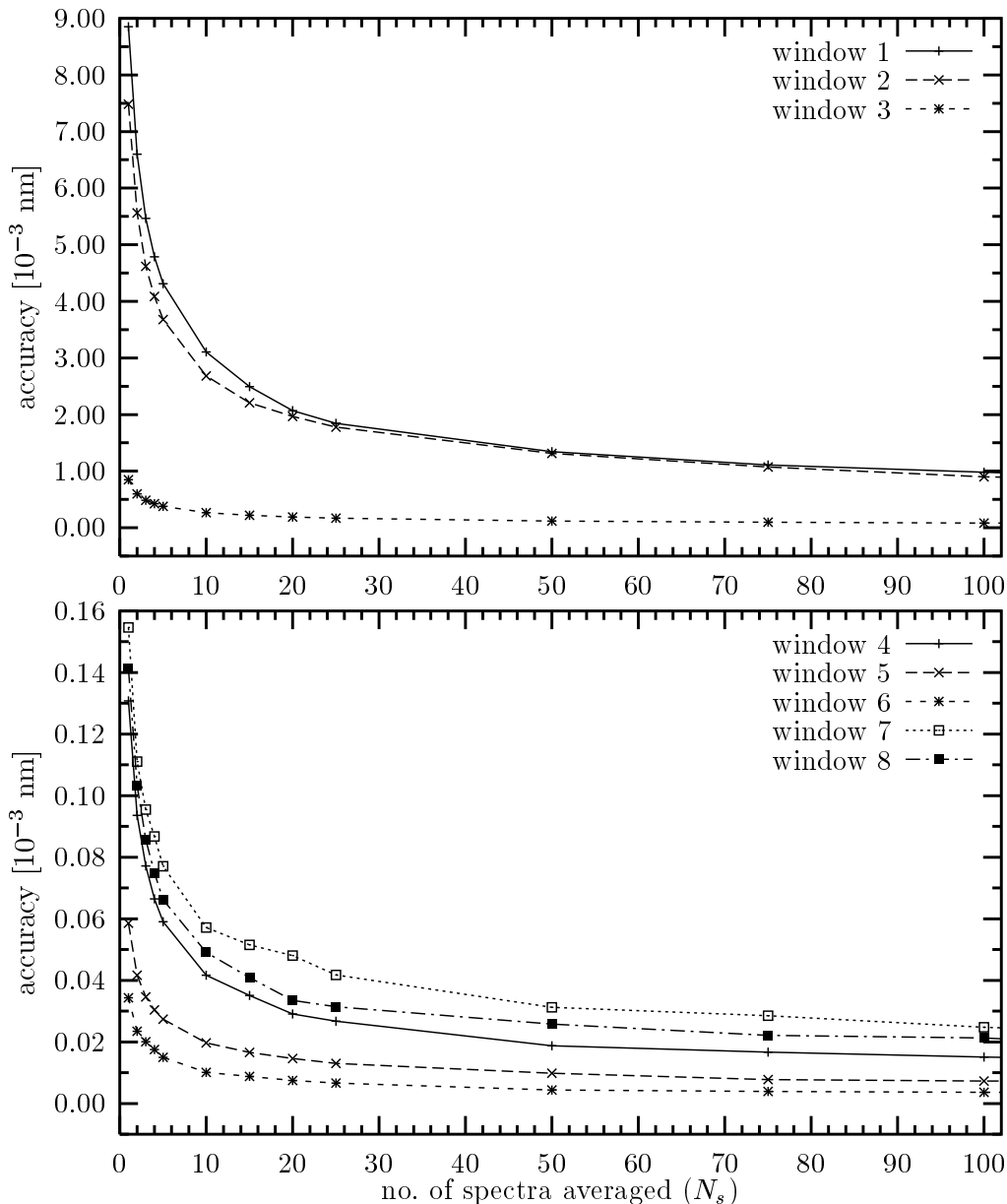


**Figure 8** Accuracy, given in  $10^{-3}$  nm, for windows 1 through 8, as function of the number of spectra averaged, determined from the simulations discussed in Section 3.5. Note the different scales in the two panels.

the number of spectra that should be averaged. Averaging over too many spectra is not advisable, as the calibration results vary along an orbit (see Section 3.7).

Figure 8 shows the accuracy as defined in Eq. (12) for the first eight windows as function of  $N_s$  in units of  $10^{-3}$  nm. Clearly, the accuracy improves with increasing  $N_s$ . Note that the calibration in windows 7 and 8 is less accurate than in windows 4–6 because windows 7 and 8 have fewer data points (*cf.* Table 2). The accuracy for window 9 is expected to be of the same order as or better than the accuracy for window 6 (Section 3.4).

For windows 1 and 2 an accuracy of 0.002 nm is reached when 20 spectra are averaged. This accuracy is of the order of the accuracy of the reference spectrum in this wavelength range (Section 2.1) and is it therefore a lower limit to the

accuracy of the calibration method. The accuracy for windows 3 through 8 is better than 0.001 nm even without any averaging of spectra. Note that since the integration time of band 1a, which contains window 1, is 12 seconds, whereas it is 1.5 seconds for the other bands (Section 1.1), a single measurement in window 1 can be considered to be an average over 8 spectra.

In the FDS level 0-to-1 processor, an average over 20 spectra for window 1 and 2 is adopted, which gives sufficient accuracy enough for the level 1-to-2 retrieval of ozone profiles. Since the wavelength grid does not vary significantly over 10 spectra (Section 3.7), an average over 10 spectra is used for the other windows, not so much to improve accuracy but to reduce computational time to keep the FDS within the constraint of the near-real time data delivery.

The daily measured GOME solar spectrum has a signal-to-noise ratio which is large enough for an accurate wavelength calibration without averaging of spectra, in that the accuracy is the same as or better than the accuracy of the calibration of earthshine spectra.

### 3.6 Systematic offset

When the measured spectrum is scaled, the difference between the GOME measured spectra and the reference spectrum is approximated by a fourth-degree polynomial, as discussed in Section 2.4. This approximation is not perfect, which leads to a small bias in the results of the wavelength calibration. This systematic bias is calculated for each window separately, with a simulated GOME solar and earthshine spectrum (*cf.* Section 3.4) for which the wavelength grid is known.

A re-calibration of the simulated spectrum, with as reference spectrum the Kurucz solar spectrum from which the simulated spectrum was determined, gives non-zero  $\Delta\lambda$ -values, because of the fourth-degree polynomial fit. These non-zero values thus represent the bias of the calibration method.

This bias is corrected for in the FDS level 0-to-1 processor. For solar spectra the wavelength change induced by the offset is very small:  $10^{-5}$  nm or less, and thus well within the accuracy of the method. The offset is somewhat larger for earthshine spectra, as the scaling for these spectra with the fourth-degree polynomial is less accurate: it amounts to a wavelength change of 0.002 nm or less, which is of the same order as the accuracy or better.

Note that when GDP level-1 spectra are re-calibrated, for example with Gome-Cal (Section 4), correcting for an offset is not possible as the user's choice of wavelength windows for the re-calibration is unknown in advance. But since the wavelength change due to the offset falls within the accuracy of the method, a correction for an offset is not very important.

### 3.7 Variation of the calibration results along orbits and in time

The wavelength calibration method has been applied to spectra measured by GOME in the nine windows listed in Table 2 to investigate the variation of the wavelength change which results from the calibration of earthshine spectra along orbits and between successive orbits over three days, and of solar spectra over a period of six years. Variations in the wavelength grid of earthshine spectra along

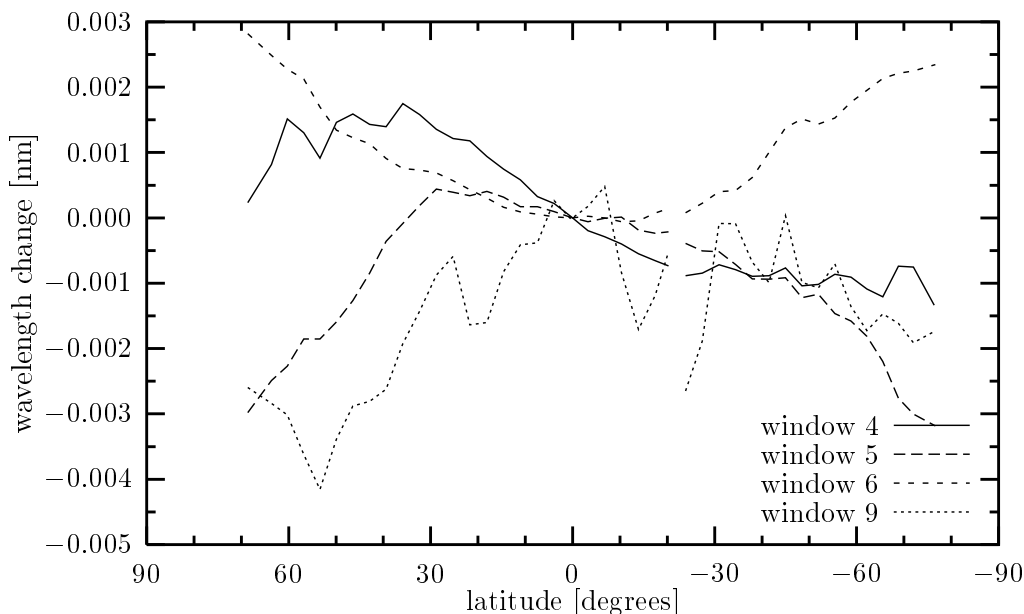


**Figure 9** Wavelength change  $\Delta\lambda(i_m)$  of the point in the middle of four selected wavelength windows, as a function of latitude. The curves have been offset with their value at the equator to configure them on a single graph. There is a gap in the curves at  $-20^\circ$  latitude because the orbit data come from two different files. Note that the accuracy of the calibration method for these windows is better than 0.0001 nm (cf. Fig. 8).

an orbit may be correlated to changes in some instrument temperatures.<sup>1</sup> A full discussion of the results of this investigation is presented in a forthcoming paper.<sup>23</sup> A few notes are in place here, in view of the averaging over spectra mentioned in Section 3.5: because of the variation along an orbit,  $N_s$  should not be too large, depending also on the desired accuracy.

For a comparison of calibration results it is essential that the initial wavelength grid from which the calibration starts is the same for all spectra used. The calibration of the FDS spectra always starts from the same initial wavelength grid (see Section 3.2) and hence that initial grid can be used.

The result of the calibration of a spectrum can be characterised by the change of the wavelength of the data point in the middle of the window:  $\Delta\lambda(i_m)$ . As the initial grid is in an arbitrary choice, the absolute value of  $\Delta\lambda(i_m)$  has no physical meaning, but the relative variation along and between orbits does. This means that  $\Delta\lambda(i_m)$  can be offset by a constant value (which may be different for each window) to make an analysis of the results easier.

Figure 9 shows, as an example,  $\Delta\lambda(i_m)$  for four selected windows along orbit 14 of 1 March 2000, where the averaging is over  $N_s = 10$  spectra. The curves in the graph show clearly that the result of the wavelength calibration varies along the orbit, and that this variation is different for different windows. For different orbits the variation along an orbit is similar, but the absolute value of  $\Delta\lambda(i_m)$  varies from orbit to orbit.

## 4. The GomeCal package: re-calibration of GDP spectra

The results of the re-calibration example in Section 3.3 and Table 4 show that the wavelength calibration of the GDP level-1 spectra can be improved; this in turn will improve the quality of the level-2 products retrieved from these spectra. The calibration method described in this paper is well suited for the re-calibration of the GDP level-1 spectra, as it can be applied to any user-specified window in any of the GOME channels.

For this purpose, a computer program has been written that reads extracted GDP level-1 data files, re-calibrates the wavelength grid and writes new level-1 data files with exactly the same format, save for the addition of a few comment lines in the file header, so that the user can see that the level-1 data file has been adapted. The next subsection describes some features of this re-calibration.

Apart from the wavelength re-calibration, two further corrections can be applied to improve GDP level-1 spectra: an improved polarisation correction<sup>24</sup> and a radiometric correction (which includes a correction for the degradation of the GOME instrument).<sup>25</sup> These corrections are described briefly in Section 4.2.

Together with supplementary programs, some examples and relevant documentation, the re-calibration program is part of the software package GomeCal, which is available on the Internet ([http://www.knmi.nl/gome\\_fd/gomecal/](http://www.knmi.nl/gome_fd/gomecal/)). The main aim of the program is to re-calibrate GDP level-1 spectra of an entire GOME orbit in one step, but a re-calibration of selected ground pixels is also possible. For more details on usage, the reader is referred to the GomeCal documentation,<sup>26</sup> which is also available on-line.

### 4.1 Wavelength re-calibration in GomeCal

The re-calibration of the wavelengths of a GDP level-1 spectrum can be done with GomeCal in any wavelength window (provided that the window is fully within a single channel). The program contains pre-selected windows, but this can be changed by the user. For example, someone interested only in ozone columns can select a single window, say 325–335 nm, perform the re-calibration only in that window and then do a DOAS-type retrieval. For each selected window the user can also specify the spectral resolution of the slit function; as noted in Section 2.3 the values given in the fourth column of Table 1 are perhaps not optimal.

The initial grid of the calibration is determined by a fit of the fifth-degree polynomial of Eq. (2) through the wavelengths in the extracted GDP level-1 file. This grid is re-calibrated in each selected window separately, as described in Section 2. The result is a new wavelength grid which is different for the different windows. In order to get a new wavelength grid for an entire channel, the new wavelength grids of the selected windows in that channel can be expanded to the full channel. If a GomeCal user is interested in a single window, then the expansion to the entire channel is not necessary.

Consider, as an example, the re-calibration of the solar spectrum measured by GOME on 1 May 1998 in channel 1. The initial grid that follows from the GDP

**Table 5** Results of the re-calibration of the GDP solar spectrum of 1 May 1998 in four wavelength windows in channel 1 with GomeCal. The second and third column give the shift and squeeze with respect to the initial grid of Eq. (13). Columns four and five give the new first and second coefficients of the wavelength grid for the window.

| wavelength window  | $\alpha$  | $\beta$  | $a_1 + \alpha$ | $a_2\beta$ |
|--------------------|-----------|----------|----------------|------------|
| 271.00 – 277.00 nm | −0.078447 | 1.002257 | 236.9918       | 0.122882   |
| 277.00 – 287.00 nm | −0.063982 | 1.001539 | 237.0062       | 0.122794   |
| 292.51 – 302.96 nm | +0.063483 | 0.999265 | 237.1337       | 0.122515   |
| 307.50 – 312.00 nm | −0.024647 | 1.000000 | 237.0455       | 0.122606   |

wavelengths is given by Eq. (2), with:

$$\begin{aligned}
 a_1 &= 237.0702, & a_2 &= 0.122605, & a_3 &= -0.259958 \times 10^{-4}, \\
 a_4 &= 0.151888 \times 10^{-7}, & a_5 &= -0.667657 \times 10^{-15}.
 \end{aligned}
 \tag{13}$$

For this example four windows are used for the re-calibration, which generates 4 pairs of coefficients ( $a_1, a_2$ ) with new values — see Table 5. The wavelengths outside these windows are not changed and hence the wavelengths of the full channel no longer form a consistent (fifth-degree polynomial) set:  $a_1$  and  $a_2$  change a few times between the channel bounds (237 and 315 nm; Table 1). To acquire a consistent new wavelength grid for the entire channel, the wavelength grids of the four individual windows are expanded to the full channel by way of a fifth-degree polynomial fit through the data points of the re-calibrated wavelength grids of the four windows and spanning all of the detectors pixels in the channel. In other words, the polynomial expansion is a combination of an interpolation between the selected windows and an extrapolation outside these windows to the channel bounds. This polynomial fit thus results in a new set of five coefficients for the full channel, which are for this example:

$$\begin{aligned}
 a_1^* &= 237.7951, & a_2^* &= 0.116292, & a_3^* &= -0.628690 \times 10^{-5}, \\
 a_4^* &= -0.103095 \times 10^{-7}, & a_5^* &= 0.113764 \times 10^{-10}.
 \end{aligned}
 \tag{14}$$

The re-calibrated grid for each separate window is the best possible grid for that window. The subsequent polynomial expansion degrades the grid somewhat for the selected windows, but the wavelength grid of the channel as a whole is improved, at least for wavelengths not too far from the selected windows. The solid line in Figure 10 shows the difference in wavelengths between the grids of Eqs. (13) and (14), *i.e.* the result of the calibration including the expansion to the full channel. The new grid of Eq. (14) is useful for wavelengths above about 260 nm, which is the wavelength lower limit used for the retrieval of ozone profiles. Below 260 nm the new wavelength grid becomes increasingly unreliable due to the extrapolation, and the change in wavelength becomes even larger than the pixel size (at 237 nm the difference is −0.72 nm). The absence of a calibration window near the lower end of the channel is the reason for the large change in the value of the first coefficient, as the fifth-degree polynomial fit is free to adjust  $a_1$ . Clearly,

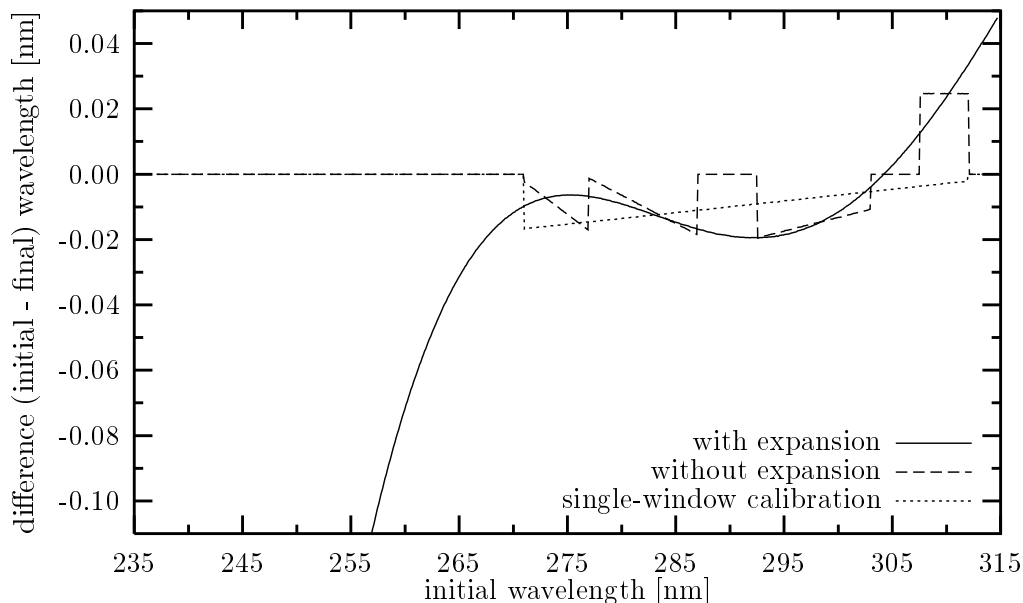


**Figure 10** Difference between the initial wavelength grid and the wavelength grid following from the re-calibration of a GDP solar spectrum in four selected windows (cf. Table 5) in channel 1 with the polynomial expansion to the entire channel (solid line; going to  $-0.72$  at  $237$  nm) and without an expansion (dashed line, where the location of the four windows can be recognised). The dotted line shows the difference when one large window is used and no expansion to the full channel is performed.

if wavelengths below  $260$  nm are needed, dedicated wavelength windows should be selected for this region in the re-calibration.

For comparison, the dashed line in Figure 10 shows the difference between the initial wavelength grid of Eq. (13) and the results for the individual windows (Table 5), *i.e.* without an expansion to the full channel, where the four individual windows can be recognised easily. Also shown in the figure is the result of a re-calibration in one large window ( $271.0 - 312.0$  nm, giving  $\alpha = 0.027961$  and  $\beta = 0.999685$ ; dotted line), which is quite different from the results using four windows.

Since the spectrum rises rather steeply from  $260$  to  $310$  nm, it is not advisable to use only one wavelength window for the re-calibration of earthshine spectra: the fourth-degree polynomial scaling of the measured spectrum (Section 2.4) cannot handle such a large variation in the radiance level with wavelength. In that sense, the broad-scale absorption features in the earthshine spectrum thus restricts the width of the wavelength windows to be selected for the re-calibration: if the window is too wide, the scaling and hence the calibration do not work well.

## 4.2 Other corrections in GomeCal

The GDP applies a correction for the polarisation of the backscattered light of earthshine spectra based on a theoretical value at  $300$  nm and polarisation measurements made in about  $100$  nm wide windows around  $350$ ,  $500$  and  $700$  nm.<sup>4,27</sup> This correction, however, appears to be insufficiently accurate, especially in the UV range, thereby causing rather large errors in *e.g.* retrieved ozone profiles. An

improved polarisation correction for the wavelength range 290–330 nm has been developed by Schutgens and Stammes,<sup>24</sup> which fully replaces the polarisation correction of the GDP extractor. This new polarisation correction has been included in the GomeCal package and it can be applied optionally to GDP level-1 spectra. Recently, Schutgens and Stammes<sup>28</sup> developed a new approach to the polarisation correction of polarisation sensitive space-borne spectrometers, such as GOME, which extends the correction to visible and near-infrared wavelengths. It is intended to implement this new polarisation correction in GomeCal at a later stage.

Another shortcoming of the GDP spectra is that the absolute calibration of the radiance is not accurate enough for the retrieval of ozone profiles. Additionally, there has been a degradation in the GOME instrument, notably since 1998, which is only partly corrected for by the GDP extractor. The degradation is time and wavelength dependent, and the measured earthshine radiance degrades differently from solar irradiance spectra. Van der A<sup>25</sup> has developed software that improves the radiometric calibration of GDP level-1 spectra, performs a correction for the degradation of the instrument, and applies a correction to remove residual effects of the interference of the Peltier cooler signals. These corrections have also been included as options in GomeCal.

## 5. Concluding remarks

The Fast Delivery Service at KNMI provides ozone and cloud information based on measurements of the GOME instrument (aboard ERS-2) on a near-real time basis, *i.e.* within three hours after observation. The Fast Delivery Service includes a level 0-to-1 processor to derive spectral information (level-1 data) from the raw (level-0) data received at KNMI for this purpose. One of the steps in this processor is a wavelength calibration, which must be accurate enough to facilitate the retrieval of reliable ozone columns and profiles. To this end, a wavelength calibration method has been developed that uses a high-resolution solar spectrum as reference spectrum and performs a combination of shift and squeeze on the spectra to derive the best wavelength grid. The accuracy of the method is about 0.002 nm for wavelengths below about 290 nm, and 0.001 nm for higher wavelengths.

The result of the calibration, that is the change of the wavelength of a point in a given window with respect to an initial guess, appears to vary along an orbit and from orbit to orbit. This obviously limits the number of spectra that can be averaged before the wavelength calibration to improve the signal-to-noise ratio of the spectrum to be calibrated. This orbital variation is discussed in a forthcoming paper,<sup>23</sup> which also investigates the change in the calibration results of solar spectra over a period of six years.

Once daily GOME measures a solar spectrum, when it flies over the North Pole into the sunlight along one of its orbits. GOME then flies towards the Sun, hence there is a Doppler-shift in the wavelength of  $\lambda v/c$ , where  $v$  is the satellite's velocity (about 8.3 km/s) and  $c$  the speed of light. This shift is between about 0.008 nm at  $\lambda = 300$  nm and 0.022 nm at  $\lambda = 800$  nm. The calibration method's fitting of a shift and a squeeze against the solar reference spectrum, automatically corrects for this Doppler-shift.

There are a few improvements possible on the calibration method. The accuracy of the reference spectrum below 300 nm, for example, could be improved upon. The reference spectrum is based on ground-based and balloon-based measurements of the solar spectrum, and it thus contains some atmospheric absorption features, over and above the distinct solar Fraunhofer lines. It is very desirable to have a pure high-resolution solar spectrum, *e.g.* measured from space, as reference for the calibration of measured solar spectra. A high-resolution earthshine spectrum as reference for measured earthshine spectra could also be useful. The use of earthshine reference spectrum, however, would introduce problems in determining how good the method works, because of the large variation in atmospheric absorption features in measured spectra. Alternatively, one could use a true solar reference spectrum and also use ozone cross sections in the fit when optimising for ozone retrieval, though the subsequent ozone retrieval itself may then no longer be independent of the wavelength calibration.

The accuracy of the method may further be improved by extending the calibration to also fit the resolution of the slit function used to convolve the high-resolution reference spectrum. This will make the method computationally slower, which is not acceptable within the constraint of near-real time delivery of the data of the Fast Delivery Service and was therefore not done. Furthermore, fitting the resolution is perhaps only useful if the slit function itself is known well, which is not the case for GOME.

The Fast Delivery Service is based on a set of nine wavelength windows plus the instrument health parameters, together known as the EGOI-data. The wavelength calibration method has been designed for these nine EGOI-windows. The method is, however, not restricted to these windows: it can be used with any set of wavelength windows within the available reference spectrum. The method is thus suitable for use with any high-resolution (ir)radiance spectrometer, such as the satellite instruments SCIAMACHY (aboard ENVISAT; launched in 2002), OMI (aboard EOS-Aura; to be launched in 2004), and GOME-2 (aboard METOP; to be launched in 2005).

The GOME level-1 spectra produced with the GOME Data Processor (GDP) have wavelength calibrations based on the spectrum of an onboard calibration lamp and a shift is applied to the spectra (no squeeze). The GDP-provided wavelength grid of the level-1 spectra appears to be insufficiently accurate for some level 1-to-2 retrievals, such as for ozone profiles. The accuracy of the DOAS-retrieval of *e.g.* ozone, BrO and NO<sub>2</sub> will also benefit from a more accurate wavelength calibration. It is therefore useful to have the possibility to improve the wavelength calibration of GDP level-1 spectra within user specified wavelength windows. For the purpose of such a re-calibration, the GomeCal software package has been written and is made available on-line via [http://www.knmi.nl/gome\\_fd/gomecal/](http://www.knmi.nl/gome_fd/gomecal/). The GomeCal package also provides an improved polarisation correction as well as an additional correction for the degradation of the GOME instrument and a radiometric calibration.

## Acknowledgements

The research described in this paper was performed within the framework of the GOME Fast Delivery and Value-Added Products (GOFAP) project, part of ESA's Data User Programme (DUP). The authors would like to thank P. Valks, R. van der A, A. Piters, P. Stammes and R. Voors for useful discussions.

## References

1. *The Global Ozone Monitoring Experiment (GOME) Users Manual* SP-1182, European Space Agency, Noordwijk, The Netherlands (1995).
2. A. Hahne, *The Global Ozone Monitoring Experiment* SP-1212, European Space Agency, Noordwijk, The Netherlands (1997).
3. J.P. Burrows, M. Weber, M. Buchwitz, V. Rozanov, A. Ladstätter-Weißenmayer, A. Richter, R. Debeek, R. Hoogen, K. Bramstedt, K.-U. Eichmann, M. Eisinger, and D. Perner, "The Global Ozone Monitoring Experiment (GOME): Mission concept and first results," *J. Atmos. Sciences* **56**, no. 2, 151–175 (1999).
4. W. Balzer, B. Aberle, D. Loyola, and R. Spurr, "GOME Level 0 to 1 Algorithm Description," *ER-TN-DLR-GO-0022*, Iss./Rev. 4/A, Deutsches Centrum für Luft- und Raumfahrt, Oberpfaffenhofen, Germany (1996).
5. A. Von Bargaen, and W. Thomas, "Updated report for GDP 0-to-1 Version 2.0 and GDP 1-to-2 Version 2.7," release by D. Loyola, *ER-TN-DLR-GO-0043*, Iss/Rev.1/A, Deutsches Centrum für Luft- und Raumfahrt, Oberpfaffenhofen, Germany (1999).
6. M. Allaart, P. Valks, R. Van der A, A. Piters, H. Kelder, and P. Van Velthoven, P., "Ozone mini-hole observed over Europe, influence of low stratospheric temperature on observations," *Geophys. Research Letters* **27**, 4089–4092 (2000).
7. P.J.M. Valks, A.J.M. Piters, J.C. Lambert, and C. Zehner, "Improved near-real time GOME ozone column retrieval," in *Proceedings of the ERS-ENVISAT Symposium: Looking down to Earth in the New Millennium*, SP-461, European Space Agency, Noordwijk, The Netherlands (CD-ROM) (2000).
8. R.J. Van der A, H.J. Eskes, J. Van Geffen, R.F. Van Oss, A.J.M. Piters, P.J.M. Valks, and C. Zehner, "GOME Fast delivery and value-Added Products (GOFAP)," in *Proceedings of the ERS-ENVISAT Symposium: Looking down to Earth in the New Millennium*, SP-461, European Space Agency, Noordwijk, The Netherlands (CD-ROM) (2000).
9. P.J.M. Valks, A.J.M. Piters, J.C. Lambert, C. Zehner, and H. Kelder, "A Fast Delivery system for the retrieval of near-real time ozone columns from GOME data." *Int. J. Remote Sensing* **24**, 423–436 (2003).
10. R.J. Van der A, A.J.M. Piters, R.F. Van Oss, P.J.M. Valks, J.H.G.M. Van Geffen, H.K. Kelder, and C. Zehner, "Near-real time delivery of GOME ozone profiles," in *Proceedings of the ERS-ENVISAT Symposium: Looking down to Earth in the New Millennium*, SP-461, European Space Agency, Noordwijk, The Netherlands (CD-ROM) (2000).
11. R.B.A. Koelemeijer, P. Stammes, J.W. Hovenier, and J.F. De Haan, "A fast method for retrieval of cloud parameters using oxygen A-band measurements from the Global Ozone Monitoring Experiment," *J. Geophys. Res.* **106**, 3475–4390 (2001).
12. R.B.A. Koelemeijer, P. Stammes, J.W. Hovenier, and J.F. De Haan, "Global distribution of effective cloud fraction and cloud top pressure derived from oxygen A band spectra measured by the Global Ozone Monitoring Experiment: Comparison to ISCCP data," *J. Geophys. Res.* **107**, 10.1029/2001JD000840 (2002).
13. A.J.M. Piters, R.J. Van der A, J.H.G.M. Van Geffen, R.F. Van Oss, and P.J.M. Valks, "Retrieving spectral reflectivities from Extracted GOME Instrument header data," in *Proceedings of the ERS-ENVISAT Symposium: Looking down to Earth in*

- the New Millennium*, SP-461, European Space Agency, Noordwijk, The Netherlands (CD-ROM) (2000).
14. P.K. Bhartia (ed.), *OMI Algorithm Theoretical Basis Document, Volume II, OMI Ozone Products*, OMI-ATBD-02, Version 2.0, NASA Goddard Space Flight Center, Greenbelt, Md. (2002).
  15. K. Chance, and R.J.D. Spurr, "Ring effect studies: Rayleigh scattering, including molecular parameters for rotational Raman scattering, and the Frounhofer spectrum," *Applied Optics* **36**, 5224–5230 (1997).
  16. C. Caspar, and K. Chance, "GOME wavelength calibration using solar and atmospheric spectra," in *Proceedings of the Third European Remote Sensing Satellite Scientific Symposium: Space at the Service of our Environment*, T.-D. Guyenne and D. Danesy (eds.), SP-414, European Space Agency, Noordwijk, The Netherlands, pp. 609–614 (1997).
  17. W.H. Press, S.A. Teukolsky, W.T. Vetterling, W.T. and B.P. Flannery, *Numerical Recipes in FORTRAN; The Art of Scientific Computing* (2nd ed.), Cambridge University Press, Cambridge, UK (1992).
  18. D.M. Stam, J.F. De Haan, J.W. Hovenier and P. Stammes, "A fast method for simulating observations of polarised light emerging from the atmosphere applied to the oxygen A band," *J. Quantitative Spectroscopy and Radiative Transfer* **64**, 131–149 (2000).
  19. A. Berk, L.S. Bernstein, and D.C. Robertson, "MODTRAN: A moderate resolution model for LOWTRAN-7," *GL-TR-89-0122*, Geophysics Laboratories, Hanscom Air Force Base, Mass. (1989).
  20. A. Berk, L.S. Bernstein, G.P. Anderson, P.K. Acharya, D.C. Robertson, J.H. Chetwynd and S.M. Adler-Golden, "MODTRAN cloud and multiple scattering upgrades with application to AVIRIS." *Remote Sens. Environ.* **65**, 367–375 (1998).
  21. R.L. Kurucz, "The solar spectrum," in *The Solar Interior and Atmosphere*, A.N. Cox, W.C. Livingston and M. Matthews (eds.), University of Arizona Press, Tucson, Ariz., pp. 663–669 (1992).
  22. R.L. Kurucz, "The solar irradiance by computation," in *Proceedings of the 17th Annual Review Conference on Atmospheric Transmission Models*, Geophysics Laboratories, Hanscom Air Force Base, Mass. (1994).
  23. J.H.G.M. Van Geffen, "Wavelength calibration of spectra measured by GOME: variations along orbits and in time," *Remote Sensing of the Environment*, to be submitted (2003).
  24. N.A.J. Schutgens, and P. Stammes, "Parametrisation of Earth's polarisation spectrum from 290 to 330 nm," *J. Quantitative Spectroscopy and Radiative Transfer* **75**, 239–255 (2002).
  25. R. Van der A, *Recalibration of GOME spectra for the purpose of ozone profile retrieval*, Technical Report TR-236, KNMI, De Bilt (2001).
  26. J.H.G.M. Van Geffen, *Documentation of the software package GomeCal* (version 1.0), Technical report TR-XXX, KNMI, De Bilt – in preparation (2003). [Also available on-line via [http://www.knmi.nl/gome\\_fd/gomecal/](http://www.knmi.nl/gome_fd/gomecal/)]
  27. R.J.D. Spurr, *Linearized Radiative Transfer Theory – A general discrete ordinate approach to the calculation of radiances and analytic weighting functions, with application to atmospheric remote sensing*, Ph.D. thesis, Eindhoven University of Technology, Chapter 5 (2001).
  28. N.A.J. Schutgens and P. Stammes, "A novel approach to the polarisation correction of space-borne spectrometers," *J. Geophys. Res.* , in press (2003).